11 Optical Properties of Correlated Electrons

Dirk van der Marel
Department of Quantum Matter Physics
Université de Genève
Quai Ernest-Ansermet 24, CH-1211 Genève 4

Contents

E. Pavarini, E. Koch, J. van den Brink, and G. Sawatzky (eds.)
Quantum Materials: Experiments and Theory
Modeling and Simulation Vol. 6
Forschungszentrum Jülich, 2016, ISBN 978-3-95806-159-0
http://www.cond-mat.de/events/correl16

1 Introduction

Optical spectroscopy is one of the most versatile spectroscopic techniques of condensed matter physics [1]. It can be used to study lattice vibrations, electronic excitations, electronic collective modes of materials and can be readily applied in the presence of magnetic fields, high pressure, low or high temperatures. Optical spectrometers exist for almost any wavelength band of the electromagnetic spectrum and span from radio-waves through THz, visible, UV to X-rays. By virtue of a high control and reproducibility various different kinds of calibration techniques permit to obtain precise absolute numbers for the constants characterizing the optical spectra of a material. This state of affairs is further improved by advances in the past decade permitting the direct measurement of the amplitude and phase of reflected signals in the THz band of the spectrum.

Many possible experimental configurations giving access to the intrinsic optical constants of materials are nowadays routinely used, including transmission, absorption, reflection, ellipsometry, and combinations thereof. We will not dwell on all these different techniques here, but give two simple examples and continue with a short summary of how from measured optical data one obtains the fundamental properties such as optical conductivity and dielectric function. If a ray of light is reflected from the surface of a material with an angle θ relative to the surface normal, the two orthogonal types of polarization of the electric field (see Fig. 1) are (i) perpendicular to the plane of reflection ("senkrecht" in German) indicated as s-polarization, and (ii) perpendicular to the plane of reflection indicated as p-polarization. For an isotropic material the reflection coefficients for these two geometries are provided by Fresnel's laws

$$r_s = \frac{\cos\theta - \sqrt{\epsilon - \sin^2\theta}}{\cos\theta + \sqrt{\epsilon - \sin^2\theta}} \quad \text{and} \quad r_p = \frac{\epsilon\cos\theta - \sqrt{\epsilon - \sin^2\theta}}{\epsilon\cos\theta + \sqrt{\epsilon - \sin^2\theta}}\,. \tag{1}$$

Note that these reflection coefficients are complex numbers. Experimentally one can measure the intensity $R = |r|^2$ of a reflected signal quite easily, but obtaining the phase is often much more difficult. One of the solutions consists of doing a so-called "ellipsometry" experiment, whereby the state of elliptical polarization of a light-ray is measured after reflection, where the incident ray is linearly polarized with a polarization being a linear superposition of s- and p-polarization. We will not dwell on the details here, but the important thing is, that this provides the ratio r_p/r_s which now *is* a complex number. An alternative method is to take advantage of the fact that $\ln r = \ln\sqrt{R} + i\phi$ where $\phi = \mathrm{Arg}(r)$, and that $\ln\sqrt{R(\omega)}$ and $\phi(\omega)$ satisfy

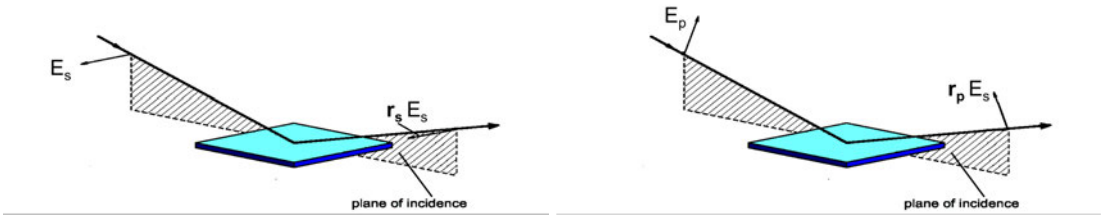

Fig. 1: *Left (right): Geometry for the reflection of s (p) polarized light.*

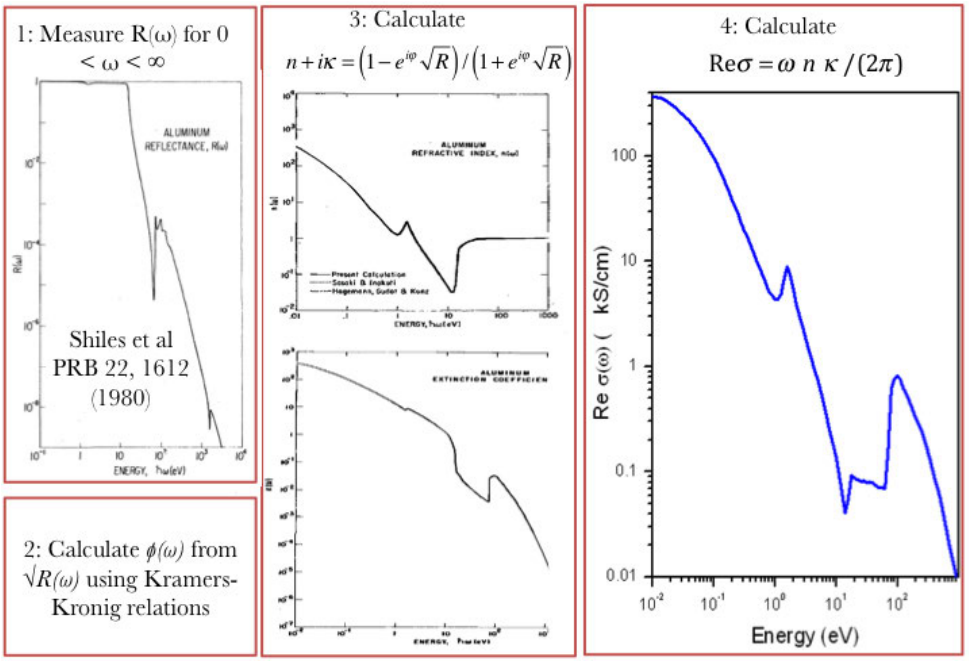

Fig. 2: *The four steps of calculating the optical conductivity from a reflectivity spectrum using the example of aluminum (after Ref. [2]).*

Kramers-Kronig relations. It is then sufficient to measure $R(\omega)$ in a sufficiently broad spectral range, in order to calculate also $\phi(\omega)$, and from these two together obtain the real and imaginary part of ϵ. This constitutes the first of the four steps providing the optical conductivity function indicated in Fig. 2 for the example of aluminum. The second is to invert the Fresnel expression for the reflection coefficient at the given angle of incidence and polarization of the light, giving as a first step the index of refraction, $n = \mathrm{Re}\,\sqrt{\epsilon}$ and the extinction coefficient $\kappa = \mathrm{Im}\,\sqrt{\epsilon}$, and from there the optical conductivity

$$\sigma(\omega) = \frac{\omega}{4\pi i}\,[\,\epsilon(\omega) - 1\,]\,. \tag{2}$$

The optical conductivity is one of the most commonly used parameters to describe the electromagnetic response. Macroscopically, the frequency dependent conductivity tensor $\sigma(\omega)$ constitutes a natural extension to the DC electrical conductivity relating electric field and current density: $\vec{j} = \sigma\vec{E}$, where $\vec{j}$ and $\vec{E}$ are the macroscopic current density and electric field components. In what follows we will assume that $\vec{j}$ and $\vec{E}$ are parallel to one of the axes of the conductivity tensor $\sigma(\omega)$, and drop explicit tensor and vector notation to keep the notation as light as possible. On the microscopic level $\sigma(\omega)$ is proportional to the current-current correlation function

$$\sigma(\omega) = \frac{e^2}{\omega V}\left\{\frac{iN}{m} + \int_0^\infty dt e^{i\omega t}\langle\psi|\,[\hat{\jmath}(t), \hat{\jmath}(0)]\,|\psi\rangle\right\}, \tag{3}$$

where N is the number of electrons, V the volume, m and e the electron mass and charge, and $\hat{\jmath}(t) = e^{iHt/\hbar}\,\hat{\jmath}\,e^{-iHt/\hbar}$ is the velocity operator. The time integral can be carried out explicitly,

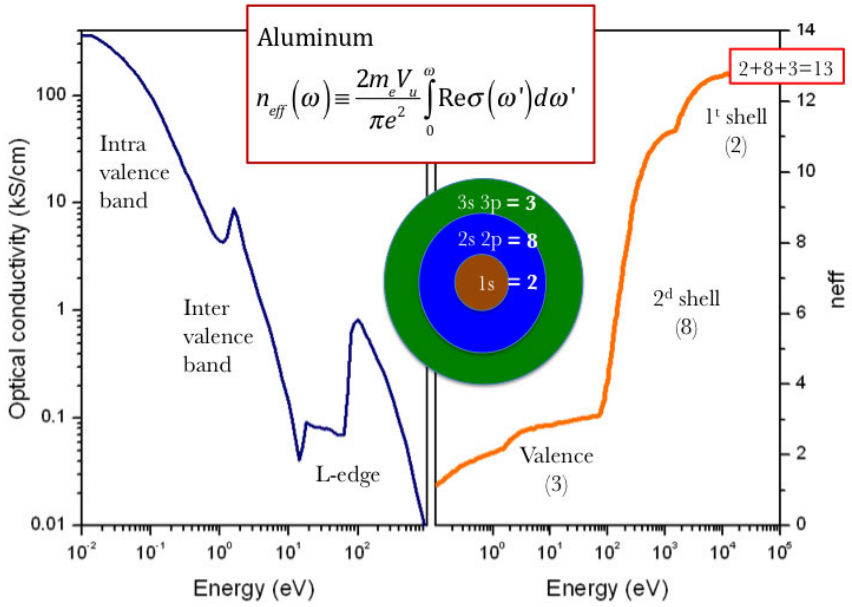

Fig. 3: *Illustration of the f-sum rule for the case of aluminum (after Ref. [2]).*

providing for the real part of the conductivity of a system in thermal equilibrium

$$\mathrm{Re}\,\sigma(\omega) = \frac{\pi e^2}{V} \sum_{\mu\nu} (Z_\nu - Z_\mu) \frac{\langle\nu|\hat{\jmath}|\mu\rangle\langle\mu|\hat{\jmath}|\nu\rangle}{E_\mu - E_\nu} \delta(\hbar\omega + E_\nu - E_\mu)\,, \tag{4}$$

where $|\eta\rangle$ is a many-body eigenstate with energy E_η and Z_η is the statistical probability to find the system in this state (the "partition function"). Integration of both sides over ω yields

$$\int_{-\infty}^{\infty} \mathrm{Re}\,\sigma(\omega)d\omega = \frac{2\pi e^2}{V} \sum_{\mu,\nu} Z_\nu \frac{\langle\nu|\hat{\jmath}|\mu\rangle\langle\mu|\hat{\jmath}|\nu\rangle}{E_\mu - E_\nu}\,. \tag{5}$$

Using $\hat{H}|\nu\rangle = E_\nu|\nu\rangle$ and $\hat{\jmath} = i\hbar^{-1}[\hat{H}, \hat{x}]$ one can show in a few steps that

$$\int_{-\infty}^{\infty} \mathrm{Re}\,\sigma(\omega)\,d\omega = \frac{\pi e^2}{i\hbar V} \langle[\hat{\jmath}, \hat{x}]\rangle\,. \tag{6}$$

At this point we can substitute on the right hand side the following useful property of the many-body current and position operators: $[\hat{\jmath}, \hat{x}] = i\hbar N/m$. We take advantage of the fact that for a time-reversal symmetric situation $\mathrm{Re}\,\sigma(\omega) = \mathrm{Re}\,\sigma(-\omega)$, so we can restrict to positive frequencies and arrive at the so-called f-sum rule

$$\int_{0}^{\infty} \mathrm{Re}\,\sigma(\omega)\,d\omega = \frac{\pi e^2 n}{2m}. \tag{7}$$

This f-sum rule, or Thomas Reich Kuhn (TRK) rule, is one of the most powerful tools in optical studies of materials. It relates the integrated optical conductivity directly to the density of charged objects, and the absolute value of their charge and mass.

In Fig. 3 the f-sum rule is illustrated by the earlier example of the aluminum: The right hand panel shows the partial integral

$$n_{\mathrm{eff}}(\omega) = \frac{2m_e V_u}{\pi e^2} \int_0^{\omega} \mathrm{Re}\,\sigma(\omega')\,d\omega'. \tag{8}$$

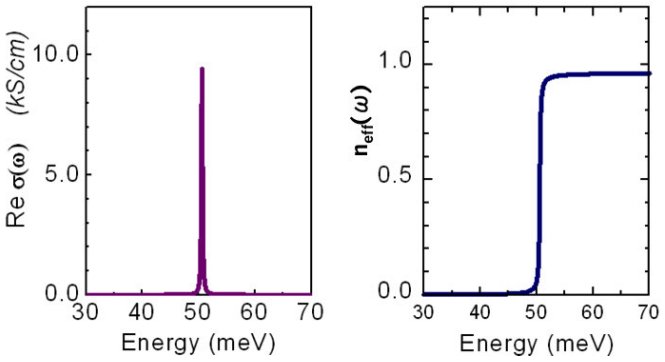

Fig. 4: *Optical conductivity and partial sumrule for the optical phonon spectrum of MgO.*

First of all it demonstrates that in the limit $\omega \to \infty$ the number $n_{\rm eff}$ approaches 13, which is exactly the number of electrons (core and valence together) per aluminum atom. Moreover, the function $n_{\rm eff}(\omega)$ rises in a number of steps: The first step from 0 to 2 eV gives approximately two electrons, from 2 to 100 eV yields an additional one, from 100 to 1000 eV adds 8 more, and above 1000 eV a final pair of electrons is added. We see, that the number of electrons in a given shell is recovered in the optical transitions from the corresponding shell to the empty states above the Fermi energy, revealing in the present example the configuration $1s^2 2s^2 2p^6 3s^1 3p^2$ (where the labels $3s$ and $3p$ are not to be taken literally in view of the lattice surrounding each Al atom). The plot also gives an impression of the scale over which one has to integrate in order to detect the spectral weight of the valence electrons: The full spectral weight corresponding to the three valence electrons is retrieved only at $\hbar\omega \approx 50$ eV.

Of course the nuclei also contribute to the f-sum rule. We left this point out of consideration until now since it usually plays a minor role, but it becomes important when analyzing the vibrational spectra of insulating materials. The f-sum rule accounting for all types of particles j with charge e_j, mass m_j and density n_j in the sample reads

$$\mathrm{Re} \int_0^\infty \sigma(\omega)\, d\omega = \sum_j \frac{\pi e_j^2 n_j}{2m_j}\,. \tag{9}$$

In Fig. 4 we show the infrared optical conductivity of the insulator MgO together with the partial sum-rule integral

$$n_{\rm eff}(\omega) = \frac{2V_u}{\pi(2e)^2(m_O^{-1} + m_{Mg}^{-1})} \int_0^\omega \mathrm{Re}\,\sigma(\omega')\, d\omega' \tag{10}$$

to illustrate that masses and charges of the Mg^{2+} and O^{2-} ions account for the spectral weight of the optical phonons. Note, however, that the spectral weight having to do with the nuclear masses is tiny as compared to the electrons. The electronic part contains some 5 orders of magnitude more spectral weight, but is not visible on this scale since the spectral range shown here is far below the band gap of this insulating material.

To provide some representative examples of the optical spectra of strongly correlated metals and insulators, we close this section with the optical spectra of the rare-earth nickelates $RNiO_3$, where R is a trivalent rare-earth ion. These transition metal compounds display a phase tran-

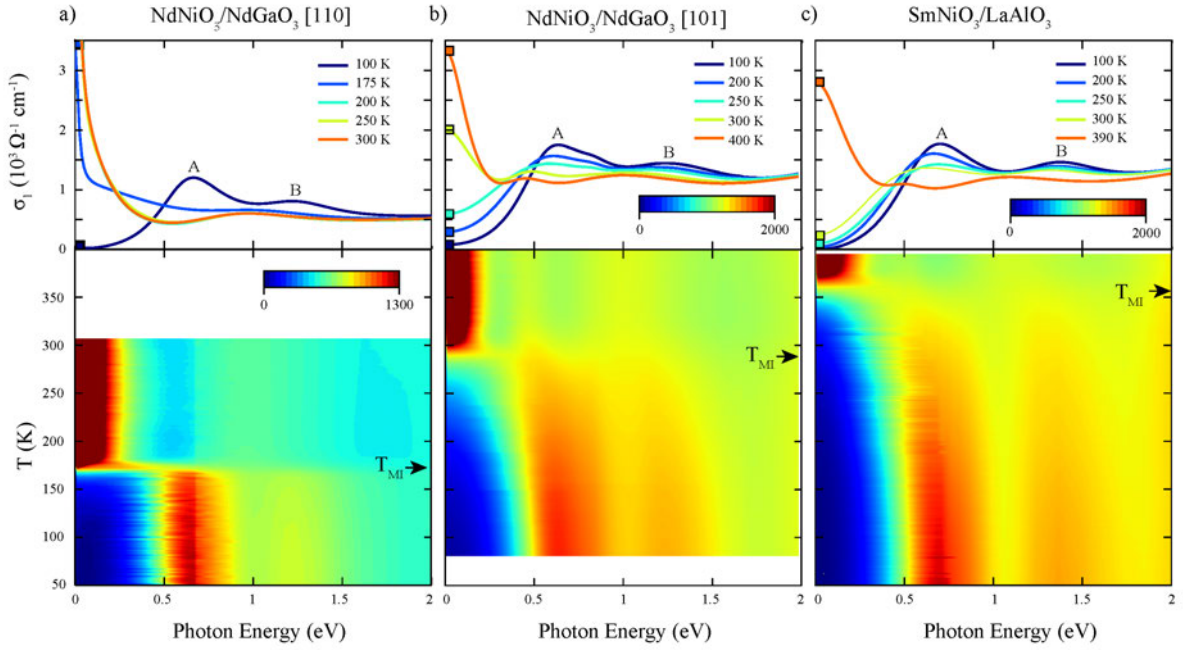

Fig. 5: *Real part of the optical conductivity for selected temperatures and energy/temperature color maps of samples (a) $NdNiO_3/NdGaO_3$-110, (b) $NdNiO_3/NdGaO_3$-101, and (c) $SmNiO_3/LaAlO_3$-001. Metal-insulator phase transitions are indicated by arrows on the color maps. A and B designate two peaks in the insulating phase (reproduced from Ref. [3]).*

sition between a high-temperature metallic phase and low-temperature insulating phases (paramagnetic or magnetic). This transition is highly sensitive to changing the rare-earth ion R, as well as structural constraints and strain. This could find applications to switches or to the recently proposed piezoelectric transistors. Furthermore strain-control can be used in order to 'orbital engineer' the nickelates, stabilizing the $d_{x^2-y^2}$ component of the e_g doublet at the expense of the d_{z^2} one. If full orbital polarization could be reached, this would lead to a 'single-band' material, with an electronic structure very similar to that of a cuprate, and hence possibly to high-temperature superconductivity. A single active band is favorable because of: (i) the absence of competing orbital fluctuations and (ii) importantly, the large antiferromagnetic superexchange expected in this case. Fig. 5 shows the energy dependence (upper panels) and energy/temperature color maps (lower panels) of the real part of the optical conductivity for three differently strain- and composition-tuned samples. In the insulating state, at low temperatures, the dominant features of the optical conductivity are two peaks at 0.6 (A) and 1.4 eV (B) for all three samples. Upon increasing the temperature and passing through the insulator-metal transition, the peaks vanish and a broad 1 eV peak along with a weak feature at 0.5 eV for samples (b) and (c) appear instead. Formation of free carriers is clearly visible with the growth of a zero energy mode in the optical conductivity for $\hbar\omega = 1$ eV (Fig. 5) as well as a sign change in the real part of the dielectric function.

The physics as to why this transition takes place is quite interesting and has been discussed in a number of recent papers. Here we quote the discussion in Ref. [3]: "Dynamical mean-field

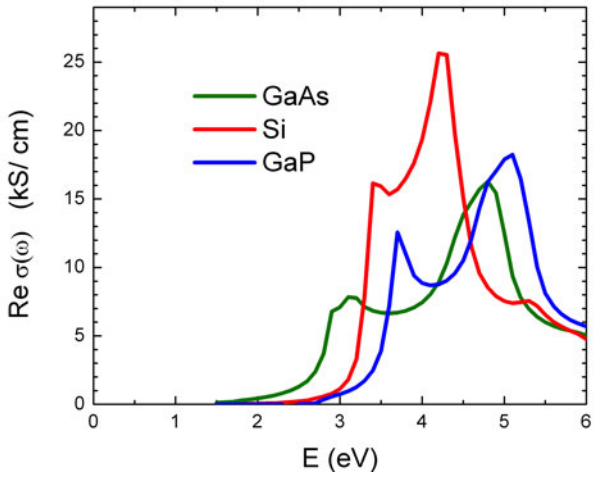

Fig. 6: *Optical conductivity of the semiconductors GaAs, Si, and GaP (after Ref. [4])*

theory calculations confirm aforementioned two-peak structure and allow us to identify these spectral changes and the associated changes in the electronic structure. We demonstrate that the insulating phase in these compounds and the associated characteristic two-peak structure are due to the combined effect of bond disproportionation and Mott physics associated with half of the disproportionated sites. We also provide insights into the structure of excited states above the gap."

2 Insulators and excitons

The example of $RNiO_3$ of the previous chapter is perhaps somewhat untypical in that the material owes its insulating gap, at least in part, to a many-body effect. In a standard semiconducting material such as GaAs the optical absorption is understood to arise from the optical excitation of individual electrons across the band gap, resulting in optical spectra such as displayed in Fig. 6. However, in many insulating materials additional absorption is observed for energies smaller than the gap, for reasons having nothing to do with impurities. The reason why this happens has to do with a fundamental issue related to the interactions between the electrons, and this shows up already when one is trying to excite a single electron. Naively one may be tempted to assume that, left by itself, a single electron should not suffer much influence of many-body effects, but this is nonetheless not justified. The problem is, that in an optical process one always creates an electron along with a hole, and these two particles interact, in fact, quite strongly. As a result, provided the electron and hole are not too far apart from each other, can (and do) form bound states, better known as excitons. The physics of excitons has much in common with that of the hydrogen atom, or rather of positronium, since both the electron and the hole have about the same mass. The fact that their masses are different coming from the fact that the electron is in the band above the gap, and the hole in the band below the gap, and the dynamical masses in these bands are usually different. The theory of exciton bound states is rather well developed. We provide a few key elements here.

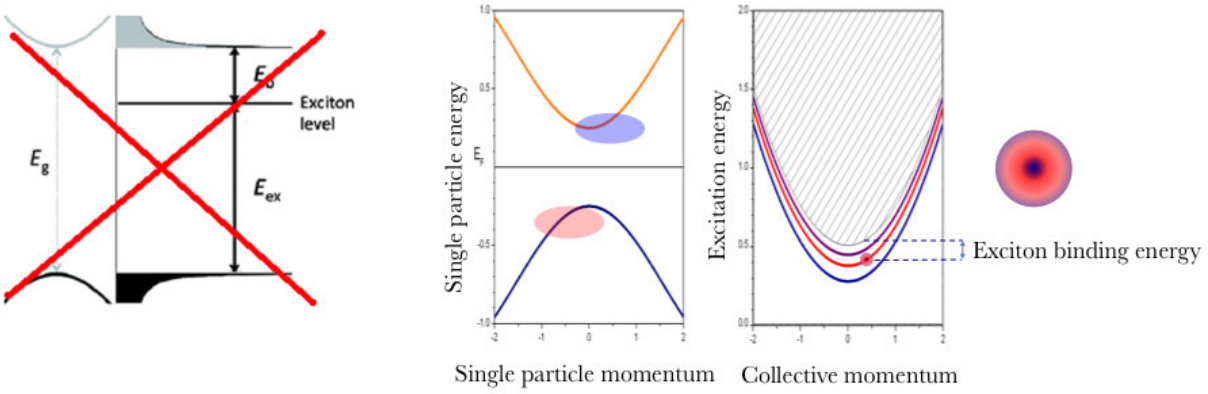

Fig. 7: *Left: incorrect way to plot the energy of an exciton. Middle panel: Sketch of the single electron dispersion curves of a direct gap insulator. Right-hand panel: Electron-hole excitation continuum corresponding to the bandstructure of the middle panel (shaded) and sketch over several "flavors" of excitons in the gap. The red and blue blobs in the middle panel indicate roughly the envelope of momentum-values involved in creating an exciton bound state with finite momentum of the collective center-of-mass coordinate.*

Quite frequently excitons are plotted in the band structure, in the way shown in the left-hand panel of Fig. 7. The difficulty is, that excitons are neutral excitations, they are bosonic, carry spin $S = 0$ or $S = 1$. Since the band-structure graph shows the energies and momenta of single-electron states, there is no unambiguous way to draw an exciton in such a diagram, and if one thinks a bit longer about the problem one realizes that by doing so one misses some important aspects of the excitonic states related to the many-body nature of these excitations, having far-reaching consequences. The middle and right-hand graphs illustrate how, as a first step, one associates electron-hole continua with a given momentum-transfer (note that only one dimension of momentum space is shown, the additional dimensions extend the number of electron-hole states for a given value of their collective momentum q shown in the right-hand panel). The electron-hole attractive Coulomb interaction can pull one or several excitonic bound states out of the continuum for any given value of q.
In the simplest description the excitons are described by the two-particle Hamiltonian

$$\begin{aligned} H &= \frac{P_{coll}^2}{2M} + \frac{p_{rel}^2}{2\mu} - \frac{e^2}{\epsilon r_{rel}} \\ M &= m_e + m_h \qquad (11) \\ \mu^{-1} &= m_e^{-1} + m_h^{-1} \qquad (12) \end{aligned}$$

so that the energies of the combined electron-hole states are described by

$$\begin{aligned} \text{Continuum states:} \quad & E_{cnt} = E_{gap} + \frac{\hbar^2 q^2}{2M} + \frac{\hbar^2 k^2}{2\mu} \\ \text{Bound states:} \quad & E_{bnd} = E_{gap} + \frac{\hbar^2 q^2}{2M} - \frac{Ry^*}{n^2} \qquad (13) \\ \text{Effective Rydberg:} \quad & Ry^* = \frac{\mu e^4}{2\epsilon^2 \hbar^2} \; . \qquad (14) \end{aligned}$$

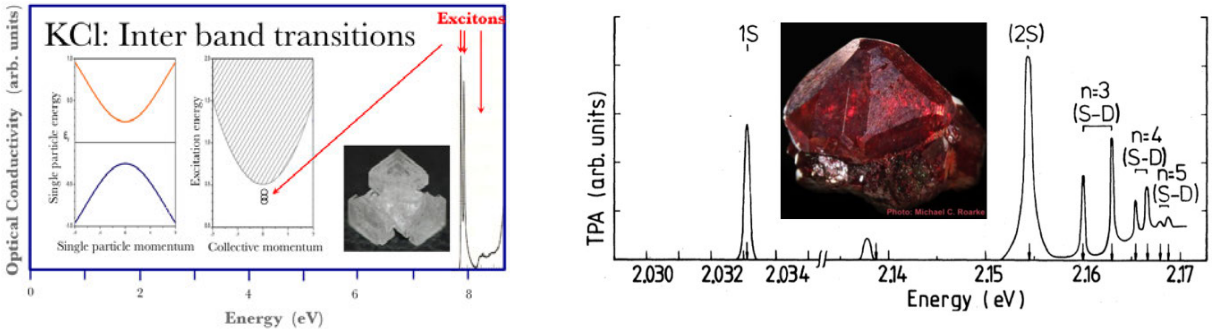

Fig. 8: *Electron-hole gap and excitonic bound states of KCl [5] and Cu_2O [6] .*

In Fig. 8 two examples are shown of simple insulating materials, with clear excitonic spectra. The left-hand graph is of KCl, having a gap of 8.5 eV, the right one of Cu_2O with a gap of and 2.17 eV. However, the single-particle bandstructure of these materials is not really described by free electron and hole parabolas, and moreover ϵ has non-trivial momentum dependence, hence the predictions of Eq. (14) can not be expected to be overly accurate, but they can provide a ballpark estimate. Indeed, the observed deepest ($n = 1$) exciton binding energies of about 0.3 eV for KCl and 0.1 eV for Cu_2O are in the right ballpark estimated from the $q = 0$ dielectric constants $\epsilon \sim 5$ for KCl, and $\epsilon \sim 7$ for Cu_2O.

Even more extreme cases of deeply bound excitons occur in Mott-Hubbard insulators, provided there is some orbital degeneracy. This is the case in, for example, $CuGeO_3$ [7] and in NiO [8,9]. In both these materials the on-site Coulomb repulsion splits apart the one-electron-removal- and one-electron-addition-states close to the Fermi-energy, with an energy separation of about 8 eV. This, in fact, pushes the one-electron removal states below the occupied oxygen band, so that the observed correlation-induced gap corresponds to the charge transfer from oxygen to Cu in the former and oxygen to Ni in the latter example. These gaps are several eV large (see Fig. 9), but a much less energy-costly excitation is possible whereby the electron-hole pair stays on the same copper or nickel site! This happens by exciting the electron from its ground state orbital

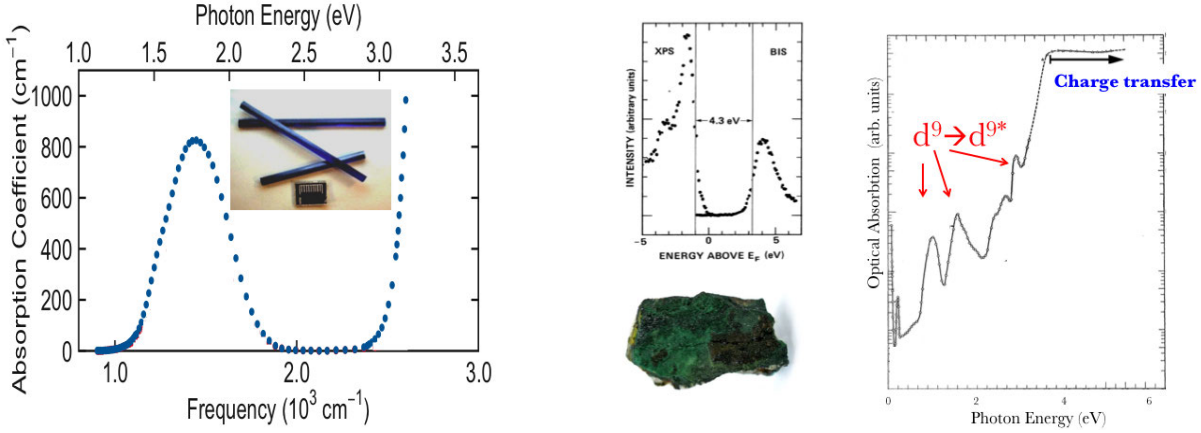

Fig. 9: *Optical spectra of the charge-transfer insulators $CuGeO_3$ [7] and NiO [8, 9], demonstrating bound neutral excitations deep inside the correlation gap.*

in the $3d$ shell to an unoccupied one. Since the electron-hole attractive interaction is of the same order as the Hubbard U, this kind of excitations (which go under the name crystal-field excitation or orbital excitation) lives deep inside the Hubbard gap. In the case of $CuGeO_3$ it gives rise to a single peak at 1.8 eV, while the charge transfer gap is about 3.1 eV. In NiO the orbital degeneracy is larger, so that a series of several peaks is observed at 1, 1.5, and 2 eV, deep inside the charge transfer gap of 4 eV.

3 Superconductors and plasmons

According to BCS theory the superconducting ground state can be described by the wavefunction

$$\begin{aligned} |\Psi_{BCS}\rangle &= \prod_k \left(u_k + v_k c^\dagger_{k,\uparrow} c^\dagger_{-k,\downarrow}\right)|0\rangle \\ |u_k|^2 + |v_k|^2 &= 1 \\ 2u_k v_k &= \frac{\Delta_k}{\sqrt{\xi_k^2 + |\Delta_k|^2}} \end{aligned} \tag{15}$$

where Δ_k is the superconducting gap. One of the most obvious and widely reported optical phenomena in a superconductor is the BCS gap. An example is shown in Fig. 10 for the conventional s-wave superconductor NbN [10].

However, in the context of superconductivity in the cuprates a number of additional effects related to superconductivity has been discovered. Here we will discuss some of these: c-axis kinetic-energy driven superconductivity has been proposed within the context of inter-layer tunneling, and has been extensively discussed in a large number of papers [11–15]. One of the main reasons to suspect that superconductivity was c-axis kinetic driven, was the observation of 'incoherent' c-axis transport of quasi-particles in the normal state [16] and, rather surprisingly, *also* in the superconducting state [17–19], thus providing a channel for kinetic energy lowering for charge carriers as soon as pairing sets in. A very useful tool in the discussion of kinetic

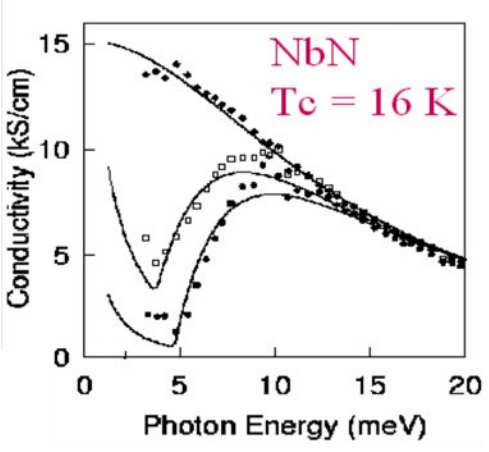

Fig. 10: *Optically detected superconducting gap of NbN*

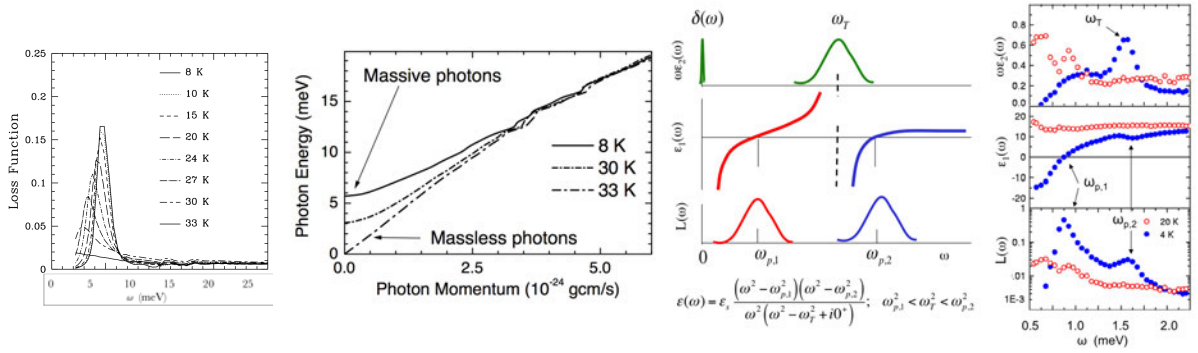

Fig. 11: *Leftmost panel: Loss-function of $La_{2-x}Sr_xCuO_4$ for field and current oriented perpendicular to the superconducting planes. The plasmon shows up in the superconducting state and is associated to the Josephson coupling between the planes. Second panel: Energy-momentum dispersion of photons polarized along the c-direction in $La_{1.85}Sr_{0.15}CuO_{4+\delta}$ for different temperatures. T_c of this sample is 33 K. The photons travelling inside the superconductor become massive, when the U(1) gauge symmetry is broken in the superconductor to which the photons are coupled. (Figure and caption copied from Ref. [20]) Third panel: Simulation of the dielectric function in a material with two types of Josephson coupling alternating [21]. Fourth (rightmost) panel: The c-axis optical conductivity and loss-function, of $SmLa_{0.8}Sr_{0.2}CuO_{4-\delta}$ for 4 K (closed symbols), and 20 K (open symbols). T_c of this sample is 16 K. When the sample enters the superconducting state, two longitudinal collective modes appear (7 and 12.8 cm^{-1}) and one with transverse polarization (12.1 cm^{-1}). The two modes near 12 cm^{-1} correspond to relative phase fluctuations of the two copper-oxygen layers within the unit cell [22]. (Figure and caption copied from Ref. [20])*

energy is the low frequency spectral weight associated with the charge carriers. In infrared spectra this spectral weight is contained within a the 'Drude' conductivity peak centered at $\omega = 0$. Within the context of the tight-binding model a simple relation exists between the kinetic energy per site, with volume per site V_u, and the low frequency spectral weight [23, 24]

$$E_{\rm kin} = \frac{\hbar^2 V_u}{4\pi e^2 a^2}\,\omega_p^2\,. \tag{16}$$

Here the plasma frequency, ω_p, is used to quantify the low frequency spectral weight

$$\frac{\omega_{p,s}^2}{8} + \int_{0^+}^{\omega_m} \mathrm{Re}\,\sigma(\omega)\,d\omega = \frac{1}{8}\,\omega_p^2\,, \tag{17}$$

where the integration should be carried out over all transitions within the band, *including* the δ-function at $\omega = 0$ in the superconducting state.

The $\delta(\omega)$ peak in $\mathrm{Re}\,\sigma(\omega)$ is of course not visible in the spectra directly. However, the presence of the superfluid is manifested prominently in the London term of $\mathrm{Re}\,\epsilon(\omega)$ (proportional to $\mathrm{Im}\,\sigma(\omega)$): $\epsilon_L(\omega) = -\omega_{p,s}^2\omega^{-2}$. In $La_{2-x}Sr_xCuO_4$ the London term is manifested in a spectacular way as a prominent plasma resonance perpendicular to the superconducting planes [25]. To illustrate this, the left-hand panel of Fig. 11 shows the so-called Loss-function

$$L(\omega) = -\,\mathrm{Im}\,\frac{1}{\epsilon(\omega)}\,, \tag{18}$$

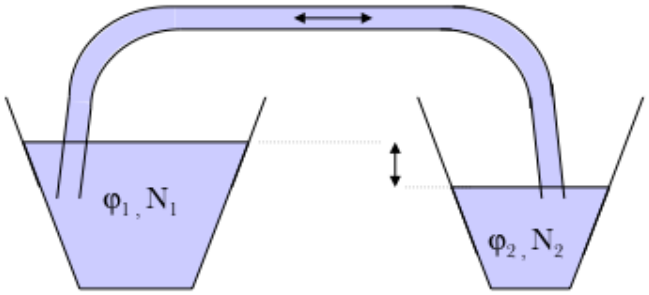

Fig. 12: *Sketch of the forces governing a Leggett mode.*

which shows its peak at the frequency where $\epsilon(\omega)$ crosses zero, which corresponds to the screened plasma-frequency. The right-hand panel shows the corresponding dispersion of the transverse polarized "polariton" waves inside the material (always with electric field perpendicular to the planes, hence the wave propagates along the planes)

$$p = \hbar\omega c^{-1}\sqrt{\epsilon(\omega)}\,. \tag{19}$$

The right-hand graph is, by the way, a nice demonstration of the Anderson-Higgs mechanism: The electromagnetic waves inside the superconductor acquire a mass $mc^2 = \hbar\omega_{p,s}$ due to the spontaneous breaking of $U(1)$ gauge symmetry associated with the superconducting order. Coupling of the superconducting order parameter to the fluctuations of charge and phase introduces a mass-gap both in the longitudinal plasmons and in the transverse polariton modes.

To return to the Josephson plasmons, a further effect was discovered when two Josephson junctions alternate along the c-direction. In this case one will observe two longitudinal Josephson plasmons, and an additional one in-between, which shows up as a peak in the optical conductivity and has transverse polarization (but always with electric field perpendicular to the planes). This was predicted theoretically and indeed observed experimentally by a number of groups. Interestingly this mode has many properties in common with the so-called Leggett mode. When in a two-band system the charge distribution is brought out of equilibrium the electronic compressibility constitutes a restoring force, whereas the inertia is given by the Josephson coupling between the two reservoirs (see sketch in Fig. 12). For a Fermi-liquid the compressibility $Kn^2 = \partial n/\partial\mu$ corresponds to density of states at the Fermi level. In the context of 'excitons' in two-band superconductors, the compressibility term has been first considered in 1966 by Leggett [26]. In neutral fluids the compressibility causes propagation of sound, whereas for electrons it causes the dispersion of plasmons.

The peak in the loss-function can be used to estimate the superfluid spectral weight, $\omega_{p,s}^2$, from the experimental spectra. Apart from universal prefactors, the amount of spectral weight of the $\delta(\omega)$ conductivity peak corresponds to the Josephson coupling energy, which in turn is the inter-layer *pair*hopping amplitude. It therefore provides an upper limit to the change of kinetic energy between the normal and the superconducting state [11], because the spectral weight transferred from higher frequencies to the $\delta(\omega)$-peak cannot exceed this amount. This allowed

a simple experimental way to test the idea of c-axis kinetic energy driven superconductivity by comparing the experimentally measured values of the condensation energy ($E_{\rm cond}$) and E$_J$. The inter-layer tunneling hypothesis required, that $E_J \approx E_{\rm cond}$. Measurements of λ_c [13] (approximately 17 μm) and the Josephson plasma resonance (JPR) [12] at 28 cm^{-1}, allowed a definite determination of the Josephson coupling energy of this compound, indicating that $E_J \approx 0.3$ μeV in Tl2201 with $T_c = 80$ K. This is a factor 400 lower than $E_{cond} \approx 100$ μeV per copper, based either on c_V experimental data [27], or on the formula $E_{cond} = 0.5N(0)\Delta^2$ with $N(0) = 1eV^{-1}$ per copper and $\Delta \simeq 15meV$. A direct determination of $E_{{\rm kin},s} - E_{{\rm kin},n}$ is obtained by measuring experimentally the amount of spectral weight transferred to the $\delta(\omega)$ peak due to the passage from the normal to the superconducting state, as was done by Basov *et al.* [14, 28]. These data indicated that for under-doped materials about 60% comes from the sub-gap region in the far infrared, while about 40% originates from frequencies much higher than the gap, whereas for optimally doped cuprates at least 90% originates from the gap-region, while less than 10% comes from higher energy.

In summary $\Delta E_{{\rm kin},c} < 0.1E_J$ in most cases. For several of the single-layer cuprates it has become clear now, that $\Delta E_{\rm kin}$ significantly undershoots the condensation energy, sometimes by two orders of magnitude or worse.

3.1 The internal energy of superconductors

The case of electrons moving in a central potential deserves our special attention: As a result of the virial theorem particles moving in a central potential of the form $V(r) = ar^n$ satisfy the relation $\langle H_{\rm kin}\rangle = \frac{n}{2}\langle V\rangle$. For an ensemble of non-interacting electrons moving in a central potential (e.g. an ensemble of hydrogen atoms) the only terms in the Hamiltonian are the kinetic energy and $V(r)$, so that the average kinetic energy is therefore a constant fraction of the average total energy, $\langle H_{\rm kin}\rangle = \frac{n}{2+n}\langle H_{\rm tot}\rangle$. The thermally induced changes of $\langle H_{\rm tot}\rangle$ are always smaller that $3k_BT$ per particle. For electrons moving in an e^2/r potential this sets an upper limit of k_BT to the change of kinetic energy, and an upper limit $4k_BT/3$ on the photon energy range over which spectral weight can be transferred as a function of temperature. From the example of a harmonic oscillator, discussed below, we will see that transfer of spectral weight as a function of temperature can even be completely absent.

A necessary condition for the existence of superconductivity is, that the free energy of the superconducting state is lower than that of the non-superconducting state. At sufficiently high temperature important contributions to the free energy are due to the entropy. These contributions depend strongly on the nature of the low-energy excitations, first and foremost of all their nature, be it fermionic, bosonic or of a more complex character due to electron correlation effects. At $T = 0$ the free energy and internal energy are equal, and are given by the quantum expectation value of the Hamiltonian, which can be separated into an interaction energy and a kinetic energy.

3.2 The Coulomb interaction energy

In a series of papers Leggett has discussed the change of Coulomb correlation energy for a system which becomes superconducting [29], and has argued, that this energy would actually decrease in the superconducting state. Experimentally the changes of Coulomb energy can be measured directly in the sector of q-space of vanishing q. The best, and most stable, experimental technique is to measure the dielectric function using spectroscopic ellipsometry, and to follow the changes as a function of temperature carefully as a function of temperature. Because the cuprates are strongly anisotropic materials, it is crucial to measure both the in-plane and out-of-plane pseudo-dielectric functions, from which the full dielectric tensor elements along the optical axes of the crystal then have to be calculated. In a recent study the evolution of the Coulomb energy was measured as a function of temperature and doping of the loss function spectra in the infrared-visible spectral range of double- and triple-layer bismuth cuprates [30]. Our experiments indicate that for the overdoped samples the superconducting phase transition is accompanied by a saving of the Coulomb interaction energy, on the underdoped side there is an increase of the Coulomb energy below T_c, and the change of Coulomb energy for $q < 0.31$ Å^{-1} is about the same size as the condensation energy. This state of affairs calls for studies with other experimental techniques, in particular electron energy loss spectroscopy, to explore the momentum dependent structure of these phenomena. Departure of a T^2 dependence of the measured loss-function data indicates a corresponding temperature dependence of the density-density correlations. Unambiguous assignment to a precursor of superconducting pairing, to another type of correlation, or neither of these two, is not possible at this stage. The S–N difference of the Coulomb energy has similar doping dependence as the total condensation energy. While the latter is in the range of 0 to 2 K per CuO_2 unit, the Coulomb energy varies between –1 and 1 K. Consequently, while it cannot be the whole cause of superconductivity, the Coulomb energy is a major factor in the total energy balance stabilizing the superconducting state. The experiments presented here demonstrate that it is in principle possible to determine the subtle changes of Coulomb correlation energy associated with a superconducting phase transition, and constitute a promising first step in the experimental exploration of the Coulomb correlation energy as a function of momentum and energy.

3.3 The kinetic energy

Based on the tight-binding approximation, a partial sum rule is sometimes employed, where the integral is limited to the valence band, excluding all other bands. Although the theoretical expressions based on the tight-binding formula are well defined, experimentalists face a problem here, due to the fact that experimentally the valence electron band overlaps with other bands, thus hindering an unambiguous separation of the various contribution in the experimental spectra. Nevertheless, relatively clear-cut cases have been reported in the literature, thus motivating us to address also the tight-binding approximation in our discussion. For a square lattice with

nearest-neighbor coupling the Hamiltonian is

$$H_{t,\alpha} = t \sum_{\vec{R},\sigma} \left(c^{\dagger}_{\vec{R}+\vec{\delta}_\alpha,\sigma} c_{\vec{R},\sigma} + c^{\dagger}_{\vec{R},\sigma} c_{\vec{R}+\vec{\delta}_\alpha,\sigma} \right) \tag{20}$$

and $H = \sum_\alpha H_{t,\alpha} - \mu N$. The commutators in Eq. (6) can be easily calculated, resulting in the f-sum

$$\int_0^\omega \mathrm{Re}\,\sigma(\infty)\, d\omega' = -\frac{\pi e^2 a^2}{2\hbar^2 V} \langle H_{t,\alpha} \rangle \,. \tag{21}$$

Note, that the chemical potential term commutes with x and drops out of the expression for the f-sum. Hence the tight-binding f-sum provides only the *kinetic energy* contribution, which depends both on the number of particles and the hopping parameter t. It is easy to see, that for a small filling fraction of the band we return to the continuum result: The occupied electron states are now all located just above the bottom of the valence band, with an energy $-t$. Hence in leading orders of the filling fraction $-\langle \psi_g | H_t | \psi_g \rangle = Nt$. Identifying $a^2 \hbar^{-2} t^{-1}$ as the effective mass m^* we recognize the familiar f-sum rule, Eq. (6), with the free electron mass replaced by the effective mass. In BCS theory the lowering of the pair-interaction energy is partly compensated by a change of kinetic energy of opposite sign. This can be understood qualitatively in the following way: The correlated motion in pairs causes a localization of the relative coordinates of electrons, thereby increasing the relative momentum and the kinetic energy of the electrons. Another way to see this, is that in the superconducting state the step of n_k at the Fermi momentum is smoothed, causing E_{kin} to become larger [31].

A pedagogical example where the kinetic energy of a pair is higher in the superconducting state, is provided by the negative-U Hubbard model [32]: Without interactions, the kinetic energy is provided by the expression

$$E_{\mathrm{kin}} = -t \sum_{\langle i,j \rangle,\sigma} \left\langle \Psi | c^{\dagger}_{i\sigma} c_{j\sigma} + H.c. | \Psi \right\rangle . \tag{22}$$

Let us consider a 2D square lattice. If the band contains two electrons, the kinetic energy of each electron is $-2t$, the bottom of the band, hence $E_{\mathrm{kin}} = -4t$. (In a tight-binding picture the reference energy is the center of the band irrespective of E_F, causing E_{kin} to be always negative). Let us now consider the kinetic energy of a pair in the extreme pairing limit, i.e. $U \gg t$, causing both electrons to occupy the same site, with an interaction energy $-U$. The occupation function n_k in this case becomes

$$n_k \approx \frac{1}{N_k} \frac{t}{U} \frac{1}{(1 + 4\epsilon_k/U)^2} \,. \tag{23}$$

This implies that the kinetic energy approaches $E_{\mathrm{kin}} \to -8t^2/U$. Hence the kinetic energy increases from $E^n_{\mathrm{kin}} = -4t$ to $E^s_{\mathrm{kin}} = -\frac{8t^2}{U}$ when the local pairs are formed. The paired electrons behave like bosons of charge $2e$. A second order perturbation calculation yields an effective boson hopping parameter [33] $t' = t^2/U$. In experiments probing the charge dynamics, this hopping parameter determines the inertia of the charges in an accelerating field. As a result

the plasma frequency of such a model would be

$$\omega_{p,s}^2 = 4\pi \frac{n}{2} (2e)^2 \frac{a^2 t^2}{\hbar^2 U} , \tag{24}$$

whereas if these pair correlations are muted

$$\omega_{p,n}^2 = 4\pi n e^2 \frac{a^2 t}{\hbar^2} . \tag{25}$$

Because the plasma frequency is just the low-frequency spectral weight associated with the charge carriers, this demonstrates, that for conventional pairs, i.e., those which are formed due to interaction energy lowering, the expected trend is, that in the superconducting state the spectral weight *de*creases. Note, that this argument can only demonstrate the direction in which the plasma frequency changes when the pair correlations become reduced, but it does not correctly provide the quantitative size of the change, since the strong coupling regime of Eq. (24) implies the presence of a finite fraction of uncondensed 'preformed' pairs in the normal state. The same effect exists in the limit of weak pairing correlations. In Ref. [34] (Eq. 29, ignoring particle-hole asymmetric terms) the following expression was derived for the plasma resonance

$$\omega_{p,s}^2 = \frac{4\pi e^2}{V} \sum_k \frac{\Delta_k^2}{\hbar^2 E_k^3} \left[\frac{\partial \epsilon_k}{\partial k} \right]^2 , \tag{26}$$

where V is the volume of the system, and $E_k^2 = \epsilon_k^2 + |\Delta_k|^2$. Integrating in parts, using that $\Delta_k^2 E_k^{-3} \partial_k \epsilon_k = \partial_k \left(\epsilon_k / E_k \right)$, and that $\partial_k \epsilon_k = 0$ at the zone-boundary, we obtain

$$\omega_{p,s}^2 = \frac{4\pi e^2}{V} \sum_k \frac{n_k}{m_k} \tag{27}$$

where $m_k^{-1} = \hbar^{-2} \partial^2 \epsilon_k / \partial k^2$, and $n_k = 1 - \epsilon_k / E_k$. For a monotonous band dispersion the plasma frequency of the superconductor is always *smaller* than that of the unpaired system: Because the sign of the band-mass changes from positive near the bottom of the band to negative near the top, the effect of the broadened occupation factors n_k is to give a slightly smaller average over m_k^{-1}, hence ω_p^2 is smaller. Note that the mass of free electrons does not depend on momentum, hence in free space ω_p^2 is unaffected by the pairing.

To obtain an estimate of the order of magnitude of the change of spectral weight, we consider a square band of width W with a Fermi energy $E_F = N_e/(2W)$, where N_e is the number of electrons per unit cell. To simplify matters we assume that $1/m_k$ varies linearly as a function of band energy: $1/m(\epsilon) = (W - 2E_F - 2\epsilon)/(W m_0)$. We consider the limit where $\Delta \ll W, E_F$. Let us assume that the bandwidth ~ 1 eV, and $\Delta \sim 14$ meV corresponding to T_c =90 K. The reduction of the spectral weight is then 0.28%. If we assume that the bandwidth is 0.1 eV, the spectral weight reduction would typically be 11.4%.

If the state above T_c is *not* a Fermi liquid, the situation could be reversed. Indeed even for the 1D Luttinger liquid $n(k)$ has an infinite slope at k_F. If indeed the normal state would have a broad momentum distribution like the one indicated, the total kinetic energy becomes lower once pairs

are formed, provided that the slope of $n(k)$ at k_F is steeper in the superconducting state. This is not necessarily in contradiction with the virial theorem, even though ultimately all relevant interactions (including electron-phonon interactions) are derived from the Coulomb interaction: The superconducting correlations involve the low energy scale quasi-particle excitations and their interactions. These *effective* interactions usually have characteristics quite different from the original Coulomb interaction, resulting in $E_c/E_{\rm kin} \neq -2$ for the low-energy quasi-particles. Various models have been recently proposed involving pairing due to a *reduction* of kinetic energy. In strongly anisotropic materials such as the cuprates, two possible types of kinetic energy should be distinguished: Perpendicular to the planes [11, 35] (along the c-direction) and along the planar directions [36–41]. Interestingly, it turns out that in underdoped samples of the cuprates the "kinetic" energy behaves oppositely to the BCS prediction (i.e. it is decreased by the N–S transition), while on the overdoped side it behaves consistently with BCS (i.e. it is increased) [42–44], which is in fact consistent with numerical calculations based on the Hubbard model and the t-J model [45, 46].

4 Conclusions

The optical conductivity is a fundamental property of solids that contains the contributions of vibrational and electronic character. Among the electronic type of excitations the intra-band and inter-band transitions, excitons, and plasmons of different types correspond to the most prominent features in the spectra. In addition multi-magnon excitations or more exotic collective modes can often be detected. The careful study of the optical properties of solids can provide valuable microscopic information about the electronic structure of solids. In contrast to many other spectroscopic techniques, it is relatively easy to obtain reliable absolute values of the optical conductivity. As a result sum rules and sum rule related integral expressions can often be applied to the optical spectra.

References

[1] D.N. Basov, R.D. Averitt, D. van der Marel, M. Dressel, and K. Haule Rev. Mod. Phys., **83**, 471 (2011)

[2] E. Shiles, T. Sasaki, M. Inokuti, and D.Y. Smith, Phys. Rev. B **22**, 1612 (1980)

[3] J. Ruppen, J. Teyssier, O.E. Peil, S. Catalano, M. Gibert, J. Mravlje, J.-M. Triscone, A. Georges, and D. van der Marel, Phys. Rev. B **92**, 155145 (2015)

[4] D.E. Aspnes and A.A. Studna, Phys. Rev. B **27**, 985 (1983)

[5] T. Tomiki, J. Phys. Soc. Jpn. **26**, 738 (1969)

[6] Ch. Uihlein, D. Fröhlich, and R. Kenklies Phys. Rev. B **23**, 2731 (1981)

[7] M. Bassi, P. Camagni, R. Rolli, G. Samoggia, F. Parmigiani, G. Dhalenne and A. Revcolevschi, Phys. Rev. B **54**, R11030 (1996)

[8] G.A. Sawatzky, and J.W. Allen, Phys. Rev. Lett. **53**, 2339 (1984)

[9] R. Newman and R.M. Chrenko, Phys. Rev. **114**, 1507(1959)

[10] H.S. Somal, B.J. Feenstra, J. Schuetzmann, D. van der Marel, J.H. Kim, Z.H. Barber, V.H.M. Duijn, N.T. Hien, A.A. Menovsky, M. Palumbo, Phys. Rev. Lett. **76**, 1525 (1996)

[11] P.W. Anderson, Science **268**, 1154 (1995)

[12] A. Tsvetkov, D. van der Marel, K.A. Morel, J.R. Kirtley, J.L. de Boer, A. Meetsma, Z.F. Ren, N. Koleshnikov, D. Dulic, A. Damascelli, M. Grüninger, J. Schützmann, J.W. van der Eb, H.S. Somal, and J.H. Wang, Nature **395**, 360 (1998)

[13] K.A. Moler, J.R. Kirtley, D.G. Hinks, T.W. Li, and Ming Xu, Science **279**, 1193 (1998)

[14] D.N. Basov, S.I. Woods, A.S. Katz, E.J. Singley, R.C. Dynes, M. Xu, D.G. Hinks, C.C. Homes, M. Strongin, Science **283**, 49 (1999)

[15] J.R. Kirtley, K.A. Moler, G. Villard, A. Maignan, Phys. Rev. Lett. **81**, 2140 (1998)

[16] S.L. Cooper, and K.E. Gray, in D.M. Ginsberg (ed.): *Physical Properties of High Temperature Superconductors IV* (World Scientific, Singapore 1994)

[17] J.H. Kim, H.S. Somal, D. van der Marel, A.M. Gerrits, A. Wittlin, V.H.M. Duijn, N.T. Hien and A.A. Menovsky, Physica C **247**, 297 (1995)

[18] D. Dulic, D. van der Marel, A.A. Tsvetkov, W.N. Hardy, Z.F. Ren, J.H. Wang, and B.A. Willemsen, Phys. Rev. B **60**, R15051 (1999)

[19] A. Hosseini, S. Kamal, D.A. Bonn, Ruixing Liang, and W.N. Hardy, Phys. Rev. Lett. **81**, 1298 (1998)

[20] D. van der Marel, Journal of Superconductivity **17**, 559 (2004)

[21] D. van der Marel, and A.A. Tsvetkov, Phys. Rev. B **64**, 024530 (2001)

[22] D. Dulic, A. Pimenov, D. van der Marel, D.M. Broun, S. Kamal, W.N. Hardy, A.A. Tsvetkov, I.M. Sutjaha, Ruixing Liang, A.A. Menovsky, A. Loidl and S.S. Saxena, Phys. Rev. Lett. **86**, 4144 (2001)

[23] P.F. Maldague, Phys. Rev. **16**, 2437 (1977)

[24] D. Baeriswyl, J. Carmelo, and A. Luther, Phys. Rev. B **33**, 7247 (1986)

[25] K. Tamasaku, Y. Nakamura, and S. Uchida, Phys. Rev. Lett. **69**, 1455 (1992)

[26] A.J. Leggett, Prog. Theor. Phys. **36**, 901 (1966)

[27] J.W. Loram, K.A. Mirza, J.M. Wade, J.R. Cooper, and W.Y. Liang, Physica C **235-240**, 134 (1994)

[28] D.N. Basov, C.C. Homes, E.J. Singley, M. Strongin, T. Timusk, G. Blumberg, and D. van der Marel, Phys. Rev. B **63**, 134514 (2001)

[29] A.J. Leggett, Proc. Natl. Acad. Sci. USA Vol. **96**, 8365 (1999)

[30] J. Levallois, M.K. Tran, D. Pouliot, C.N. Presura, L.H. Greene, J.N. Eckstein, J. Uccelli, E. Giannini, G.D. Gu, A.J. Leggett, and D. van der Marel, arXiv:1512.00672

[31] M.R. Norman, M. Randeria, B. Janko, J.C. Campuzano, Phys. Rev. B **61**, 14724 (2000)

[32] R. Micnas, J. Ranninger, and S. Robaszkiewicz, Rev. Mod. Phys. **62**, 113 (1990)

[33] P. Nozières, and S. Schmitt-Rink, J. Low Temp. Phys **59**, 195 (1985)

[34] D. van der Marel, Phys. Rev. B. **51**, 1147 (1995)

[35] S. Chakravarty, Eur. Phys. J. B **5**, 337 (1998)

[36] J.E. Hirsch, Physica C **199**, 305 (1992)

[37] S. Alexandrov and N.F. Mott: *High Temperature Superconductors and Other Superfluids* (Taylor and Francis, 1994)

[38] V. Emery and S.A. Kivelson, Nature **374**, 4347 (1995)

[39] F.F. Assaad, M. Imada, and D.J. Scalapino, Phys. Rev. Lett. **77**, 4592 (1996)

[40] P.A. Lee, Physica C **317**, 194 (1999)

[41] P.W. Anderson, Physica C **341-348**, 9 (2000)

[42] H.J.A. Molegraaf, C. Presura, D. van der Marel, P.H. Kes, M. Li, Science **295**, 2239 (2002)

[43] G. Deutscher, A.F. Santander-Syro, and N. Bontemps, Phys. Rev. B **72**, 092504 (2005)

[44] F. Carbone, A.B. Kuzmenko, H.J.A. Molegraaf, E. van Heumen, V. Lukovac, F. Marsiglio, D. van der Marel, K. Haule, G. Kotliar, H. Berger, S. Courjault, P.H. Kes, and M. Li, Phys. Rev. B **74**, 064510 (2006)

[45] E. Gull and A.J. Millis, Phys. Rev. B **86**, 241106 (2012)

[46] K. Haule and G. Kotliar, Europhys. Lett. **77**, 27007 (2007)